Structural Modeling and Dynamic Analysis of Condensate Storage Tanks in Nuclear Power Plants

Jinsong Fan, Jieun Hur, Halil Sezen, Richard Denning, and Tunc Aldemir

The Ohio State University, Columbus, OH 43210 USA

Abstract:

Condensate storage tanks (CSTs) in nuclear power plants (NPPs) are classified as critical equipment capable of surviving strong shaking in a design basis earthquake to assure the ability to subsequently provide cooling water. Structural modeling and dynamic analysis of CSTs are complicated due to fluid-structure interaction (FSI) and coupling issues, which could have significant effects on seismic response. The capability of a number of approximate models to capture seismic response is investigated using dynamic analysis results from detailed finite element models. Modal analyses and time history analyses are carried out using both 2D and 3D models to predict the dynamic behavior of CSTs as a function of ground motion intensity. Although 2D simplified models can be used to quickly evaluate the dynamic response of CSTs when there is substantial margin to failure, a detailed 3D model is required when it is necessary to examine a limit state associated with the failure mode of the tank. The results show good agreement between the natural frequencies of convective modes determined from the 2D and 3D CST models. The difference between the frequencies of impulsive modes were found to be equal to or less than 25%.

Key words: Condensate storage tanks (CSTs); Nuclear power plants (NPPs); Fluid-structure interaction (FSI); Structural dynamics, Modal analysis; Time history analysis.

1. Introduction

Condensate storage tanks (CSTs) are important structures that temporarily store condensed steam before going into the steam generator after it returns from the turbine in a pressurized water reactor (PWR) or back into the reactor core in a boiling water reactor (BWR). CSTs are classified as critical safety-related equipment because, in addition to their role in the normal operation of a nuclear power plant (NPP), they also play an essential role in removing decay heat from the plant in an accident, including an accident initiated by a seismic event.

For the assessment of NPP vulnerability to seismic events, probabilistic risk/safety assessment (PRA/PSA) studies need to be conducted to estimate the likelihood and the severity of the damage following the seismic event. Recent approaches to PRA/PSA have proposed to conduct PRA/PSA for external event initiators such as earthquakes, hurricanes, tsunamis, tornados in a seamless fashion with internal event initiators (e.g. turbine trip, transients without scram) (Sezen et. al., 2019). Often called dynamic PRA (DPRA) methods (Aldemir, 2013), such seamless approaches require thousands (and often tens of thousands) simulations of the plant response to the external event which in turn require the use of simplified models of plant behavior for computational feasibility. The objective of this paper is to investigate the validity of using simplified models for CSTs for DPRA following a seismic event.

A pair of redundant CSTs are illustrated adjacent to an auxiliary building of a hypothetical PWR in Figure 1 (Sezen et al., 2015). Although industrial standards and design guidance have been established for CST facilities (ACI 350.3, 2006; API-650, 2007; Eurocode 8, 2006; NZS3106, 2010), there is no uniformly accepted procedure to perform dynamic analysis of large CSTs under seismic loading. As part of the DPRA process, seismic probabilistic risk assessment (SPRA) necessitates use of seismic loads that are substantially larger than those used to establish the design bases of seismic events for the plant. CSTs could be considerably damaged or functionally failed during strong earthquakes greater than the design-basis ground motion. For example, according to an investigation after a major earthquake in Alaska in 1964 (National Research Council U.S., 1968), many tank structures suffered significant damage including pipe leaking, buckling of structural walls, and anchorage failures. Because of the cost associated with the modeling and combined structural-hydraulic finite element (FE) analysis of large water tanks, the development of reliable faster-running approximate models would be of value, particularly for the performance of uncertainty analyses for which large numbers of scenarios are examined.

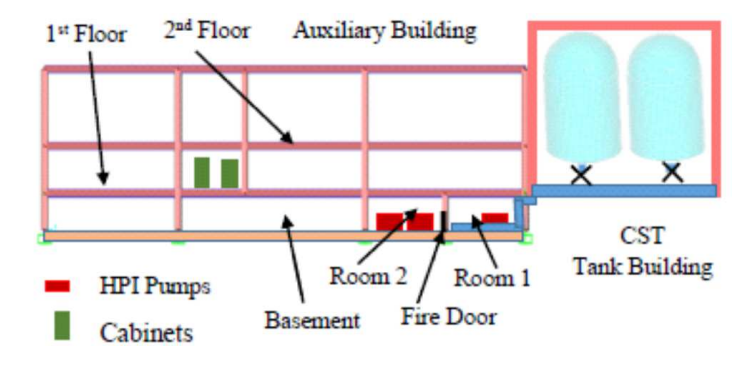


Fig. 1. Condensate storage tank location in nuclear power plant system

Earlier studies focused more on the storage tank body design, strength evaluation and failure using simple analytical models (Veletsos and Yang, 1977). The seismic evaluation of CSTs requires prediction of natural frequencies, hydrodynamic pressure distribution on tank walls, base shear and overturning moments as well as free surface movements of the contained fluid, which have direct impacts on the dynamic behavior of CSTs excited by an earthquake. A number of simplified CST models were proposed based on previous research efforts (Housner, 1963; Bauer, 1964; Haroun and Housner, 1981; Veletsos, 1984). Some of these models were adopted in engineering practice and incorporated into design codes, and manuals (EPRI 6041, 1991; EPRI TR-103959, 1994; ACI 350.3, 2006). Jiswal et al. (2008) conducted a series of experiments and numerical analyses to figure out sloshing frequencies of simplified square tanks with centrally placed obstructions. Mandinscak (2009) also studied about the impact of flexibility of square tanks on sloshing behavior. Both studies considered the square shaped tanks with sinusoidal force/displacement to observe fluid-structure interaction. For the present study, we are using the actual seismic ground motion histories to determine the CST response in NPPs.

The tank structure model is typically assumed to be fixed to the foundation and acts like a cantilever column. The tank system is treated as a single-degree or two-degree freedom system in terms of the lateral displacement of CSTs within the horizontal plane. However, unlike ductile solid steel structures, partially liquid-filled tanks have an additional mechanism to dissipate seismic energy. In earlier studies, a simplified circular tank model was first proposed by Housner (1963) with a rigid wall assumption. Wozniak and Mitchell (1978) examined the cases for short and slender tanks based on the Housner's model.

During strong earthquakes, flexible tank walls may deform significantly and experience stresses larger than that of identical cases with rigid tank walls. Subsequent experimental and analytical studies demonstrated that the flexibility of the tank walls has a strong effect on the dynamic response of a tank. Veletsos and Yang (1977) indicated that the flexibility of the shell can cause the contained liquid movement to intensify several times greater than the input excitation acceleration. Veletsos (1974) revealed that the predictions of base shear and overturning moments in tanks by assuming rigid shells were unreliable as evidenced by dynamic stresses greater than those obtained from rigid tank models. Consequently, Haroun and Housner (1981) and Veletsos (1984) developed mechanical models for flexible tanks. Malhotra et al. (2000) further simplified the flexible tank model created by Veletsos (1984) and demonstrated that the prediction of the hydrodynamic pressure is highly dependent on the wall flexibility.

The dynamic behavior of CSTs is governed by the coupling between the motions of the tank body and fluid inside. Fluid-structure interaction (FSI) is particularly significant when the fluid is incompressible, and the deformation on the structure wall cannot be neglected. There are several design methods that incorporate basic principles regarding the seismic behavior of the fluid-structure system (Dash and Jain, 2007; Nicolici and Bilegan, 2013). Mechanical models have been created for the fluid-tank system that incorporates simplified approaches to FSI modeling. The fluid inertial effect was represented by means of a concentrated fluid mass. For a partially-filled

tank, the fluid inside can be represented dynamically by two uncoupled concentrated masses, respectively known as impulsive and convective masses (Housner, 1963).

In the seismic design of CSTs, the capacity to resist buckling is another critical consideration because buckling of the tank wall can lead to substantial deformation of the wall. A number of FE models were developed for the analysis of tanks containing fluids. Balendra et al. (1982) used a direct FE method for studying the dynamic pressure range along flexible tank walls with independent variables designated for the fluid domain. Zou and Kong (2000) used a simplified model to examine the extent of damage experienced by cylindrical steel tanks in historically significant earthquakes. Similarly, Carluccio et al. (2009) analyzed a liquid storage tank subjected to different earthquake ground motions. The fluid inside was modeled using a fluid element defined only by a bulk modulus in order to couple the structure with the fluid through contact elements (Hur et al., 2016b). However, none of the detailed FE models incorporating coupled response of the tank structure and internal fluid has yet been incorporated into common engineering practice or design codes due to the complex nonlinear analysis and computational expense.

With the objective of improving the seismic safety and reducing the risk of damage or failure of thin-walled cylindrical liquid storage tanks, it is necessary to develop reliable seismic response analysis methods. As indicated earlier, the motivation of this paper is to investigate the dynamic behavior of CSTs (see Section 2.3) under seismic events (including the flexible walls, FSI, and hydrodynamic pressure distribution) and compare the results obtained from simplified models (Section 2.2). Industry standard FE-based programs were used in the study to predict the response of the seismically excited CSTs (Section 3). Models of varying complexity were developed from the 2D simplified to 3D comprehensive FE models using SAP2000 (2016) and ANSYS Mechanical (2017) Dynamic modal and time history analyses were performed and compared for the different models to predict failure modes (Section 4). Section 5 investigates the effect of different factors such as mesh size (Section 5.1) and ground motion magnitude on the dynamic response of the 3D CST model (Section 5.2). Section 6 summarizes the conclusions of the study.

2. Development of CST Models

This section presents how to develop FE models of CST. Section 2.1 provides the description of the representative CST including dimensions and materials. Sections 2.2 and 2.3 introduce how to generate simplified 2D models and detailed 3D models, respectively.

2.1 Representative CST

For the design characteristics of a CST representative of those in NPPs, this study used the geometric and material properties of the CST model from Nie et al. (2012) (Figure 2). The design information is summarized in Table 1. This steel CST has the shape of a vertical cylinder topped with a dome and filled with homogeneous and uniform viscoelastic fluid up to a height of h_w . For the simulation models, the tank is assumed to be fully anchored and fixed to a rigid ground.



Fig. 2. Condensate storage tanks adopted for analysis in this study (Nie et. al., 2012)

Table 1. Geometric and material properties of representative CST structure

Geometric properties				
Tank height to dome (m)	h_t	11.43		
Height of stored water (m)	h_w	10.67		
Inner radius of circular tank (m)	R_t	7.62		
Thickness of tank wall (mm)	t_s	12.70		
Thickness of tank dome (mm)	t_d	12.70		
Material properties				
Elastic modulus of steel (GPa)	E_s	200		
Yield strength of steel (MPa)	σ_{ye}	250		
Bulk modulus of water (GPa)	K	2.16		
Density of steel (m ³)	$ ho_{\scriptscriptstyle \mathcal{S}}$	7,800		
Density of fluid (water) (m ³)	ρ_w	1,000		
Poisson's ratio of tank wall	ν	0.30		

For the simulation of CSTs, three sets of simplified CST models were developed using SAP2000 (2016) based on the data given in Table 1. The models were analyzed to determine their dynamic characteristics, and the results were compared to a 3D detailed FE model implemented with ANSYS Mechanical (2017).

2.2 Simplified Models

Typical structures in NPPs can be modeled in different ways such as simplified lumped mass models, 2D and 3D FE models. Among various mechanical models created for fluid-tank system, the most popular are an equivalent two-mass model (Housner, 1963) and a three-mass model (Haroun and Housner, 1981). They are able to predict the dynamic behavior of CSTs and are widely used for analyses and design purposes.

The early studies on the dynamic or seismic behavior of CSTs have only adopted the rigid wall hypothesis (Housner, 1963). Under seismic loading, tank walls and internal fluid are subjected to horizontal acceleration. In a CST partially filled with water, the motion of the tank wall excites the fluid into oscillations that result in a dynamic force on the tank body. This dynamic force can be

approximated and modeled using a lumped inertial-mass. In the lower region of the tank, the fluid behaves like a concentrated mass that is rigidly connected to the tank walls. This mass is termed as impulsive mass which accelerates along with the tank wall and induces impulsive hydrodynamic pressure along the tank wall and bottom plate. In the upper region of the tank, the fluid mass is excited by sloshing motion. This mass is known as convective mass and thus generates convective hydrodynamic pressure on tank walls.

If the flexibility of the tank wall is considered, a part of fluid mass moves independently while the remaining part accelerates back and forth with the tank as a whole. Housner (1963) developed a simplified procedure for predicting dynamic fluid behavior in rigid rectangular and cylindrical tanks. Many current standards and guides such as ACI 350.3 (2006) have employed Housner's model for seismic design with some modifications. Later, Housner's simplified tank model was modified to account for the flexibility of the tank wall. Veletsos and Yang (1977) used one mass for the impulsive component and two convective masses in a simplified beam-behavior model. Furthermore, Haroun and Housner (1981) proposed a model to evaluate the seismic response of storage tanks including wall flexibility. In this model, a part of fluid inside moves independently from tank walls, while another part of the fluid oscillates in unison with the whole tank. Bauer (1964) subdivided impulsive mass into two subsets: one part rigidly connected to the base plate and the other part integrated into the convective mass participating in the free movement due to the deformation of the tank wall. Sezen et al. (2008) developed a simplified three-mass model and a FE tank model to carry out the dynamic analysis including the interaction effect of liquid and structure.

An idealized plane roof CST is modeled in 2D in Figure 3(a). Figures 3(b) and 3(c) illustrate two alternative simplified approaches to modeling the response of the CST. The contained fluid mass is lumped separately as convective and impulsive masses. In Figure 3, m_i and m_c denote impulsive and convective masses of fluid, respectively. m_{c1} and m_{c2} are sub-masses of convective mass. The height h_i is where the resultant of impulsive pressure on the wall is applied, while h_t and h_w are the total height of the CST wall and internal water level, respectively. Similarly, h_c is the height where the resultant of convective pressure on the wall is applied, while h_{ci} are specified as heights at which the resultant of convective pressure on the wall and the base are located. The inner radius of the CST is denoted as R_t and the thickness of tank wall is t_s . The stiffness values of the springs, k_c and k_{ci} , to correspond to the i_{th} convective mass of the fluid.

Two of the simplified 2D CST models are analyzed in this study. One is Housner's model (1963) developed with one impulsive mass and one convective mass (Figure 3(b)), and the other is the simplified model by Haroun and Housner (1981), (Figure 3(c)), which has one impulsive mass and two convective masses. In these 2D models, the impulsive masses are connected with rigid beam elements, while convective masses are connected with linear spring elements as shown in Figures 3(b) and 3(c). The CST properties are provided in Table 1 and model stiffness and mass values are calculated as described in earlier models of Housner (1963), Bauer (1964), Haroun and Housner (1981), and Hur et al. (2016b).

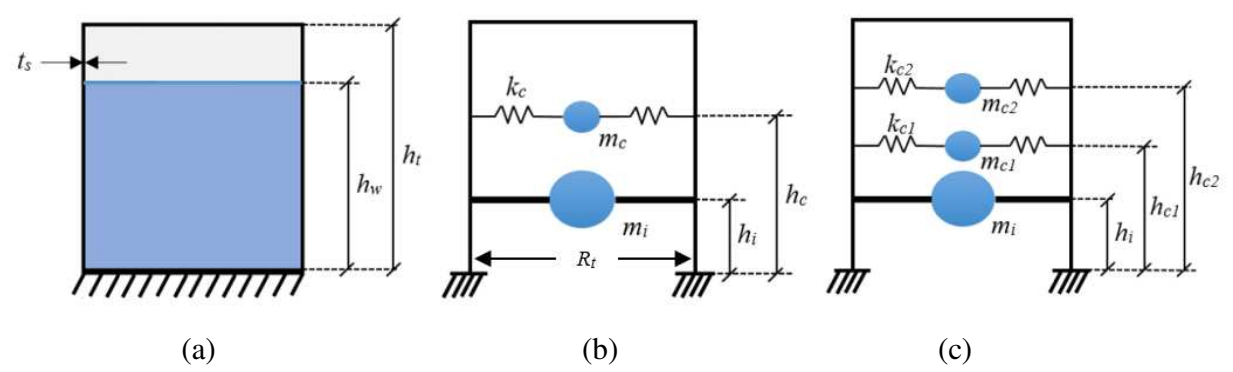


Fig. 3. Simplified 2D CST models of (a) CST profile, (b) Housner model (1963), and (c) Haroun and Housner model (1981)

2.3 Detailed 3D Models with FSI

Seismic analysis of CSTs is complicated and challenging due to the complexity of coupling effects between fluid and tank structure. More specifically, the dynamic behavior of CSTs is significantly affected by the interaction between the contained fluid and flexible tank walls. In partially filled CST system, coupling occurs on domain interfaces via the boundary conditions. Thus, the FSI effects need to be considered for seismic assessment of CSTs.

In general, FSI is defined as the interaction of movable or deformable structures with an internal or surrounding fluid flow. There is a transfer of energy from fluid to the solid and vice versa. FSI becomes particularly critical when the fluid inside is almost incompressible and deformation on the structure cannot be neglected. The Lagrangian approach, in which the reference frame moves with the fluid, has been employed in numerical solutions of fluid kinematics formulations in terms of displacements (Wilson and Khalvati, 1983). Meanwhile, the compatibility and equilibrium conditions must be satisfied at the fluid-structure interface. In FE modeling, the whole CST system can be divided into the fluid domain and shell structure domain, where a fluid domain and a tank shell domain are defined through boundary conditions, as shown in Figure 4(a). The two domains need to be discretized with the types of elements that are available in FE programs. The FSI occurs along the interface of the two domains. According to the FSI mechanism, fluid forces are applied onto the structure and the deformation changes the boundary of the fluid domain as well.

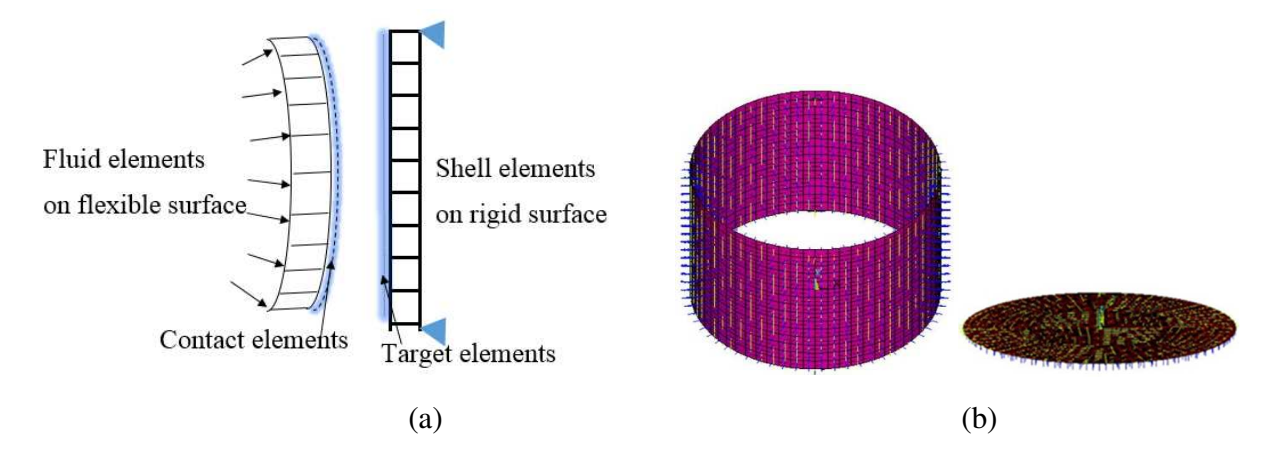


Fig. 4. FSI configuration of (a) contact pairs, and (b) contact elements on the wall and bottom of tank structure

The FSI considered in FE modeling can be achieved by setting up the contact pair along the fluid-wall interface. The contact pair plays an important role of providing coupling effects between the fluid and structure domains. Technically, a contact pair is composed of contact elements attached on one domain with more flexibility and target elements belonging to a rigid side as illustrated in Figure 4(a). The fluid elements at the wall boundary are not attached directly to the shell elements but have separate, coincident nodes that are coupled only in the direction normal to the interface. Relative movements in the tangential and vertical directions are allowed to happen at the interface. At the base, fluid element nodes are allowed to move on the surface of the CST bottom plate. In this study, no penetration behavior is allowed to occur on the two-domain interface. The structure and fluid of the 3D CST model are meshed in a way that the location of each node of the fluid domain on the interface coincides exactly with that of the corresponding shell element. Moreover, the coincident nodes are coupled in the direction normal to the fluid-structure interface, which enforces equal displacements in the radial direction for both fluid and shell nodes.

The FSI modeling and analysis in this paper are performed using the commercial program ANSYS Mechanical (2017), which is widely used for simulating coupled systems that involve structure and fluid interaction. Among available elements in ANSYS program, contact pairs are applied at the wet surface of the wall as well as at the bottom of the tank as shown in Figure 4(b). The 3D target element, TARGE170 of ANSYS with eight nodes in three degrees of freedom (DOFs) is attached on shell elements to define the boundary of the deformable body (ANSYS, 2017). In addition, CONTA174 of ANSYS is selected as the contact element between the target surface and a deformable surface. CONTA174 has three DOFs at each node and is located on the surfaces of shell elements (ANSYS, 2017). Kinematic constraints are placed on the nodes of the shell elements between the tank and the fluid and thus act as an equivalent friction force between the fluid and the tank.

It is assumed in this research that the tank bottom is rigidly attached to a rock foundation, thus the effect of uplift pressure is ignored. For the tank modeling, shell elements (SHELL181 in ANSYS) are used to take into account the membrane and bending effects of tank walls. This enables the application of normal pressures on internal surface and tangential stress on the contact interface. The 3D element SHELL181 is well suited for analyzing thin shell structures since it combines the membrane action and bending and has six DOFs per node. The fluid domain is modeled by a 3D iso-parametric fluid element of ANSYS, FLUID80 that has three DOFs at each of eight nodes. This fluid element, FLUID80 is appropriate for calculating hydrostatic pressure and considering FSI and acceleration effects, such as sloshing motion (Li et al., 2011). FLUID80 enables the simulation of three-dimensional fluid material contained in a tank. The fluid element represents water with mass density (ρ) of 1000 kg/m³ and bulk modulus (E_{ν}) of 2.067x10⁹ Pa. This water element is considered as real compressible fluid, and its coefficient of viscosity is assumed as zero.

The reliability of the simulations and analysis results of FSI depend on the application of the appropriate boundary conditions between the tank shell and fluid domains. More specifically, the free surface movement incorporating linear wave theory under dynamic loading is allowed for the

simulation of sloshing effects on the top fluid surface. The accuracy of analysis results and computational efficiency also depend on the number and size of finite elements in the model. The mesh size and the generation of finite elements are based on the range of the width of the circumferential tank wall and base plate. In order to achieve a reasonable mesh size for the dynamic analysis, the length of tank wall is divided into 20 elements in lateral direction. The tank wall parallel to the vertical direction under the roof part is divided into 15 elements. The meshed 3D CST body and fluid are shown in Figure 5. The CST model details, mesh sensitivity analysis, and dynamic analysis results are provided in Fan et al. (2017).

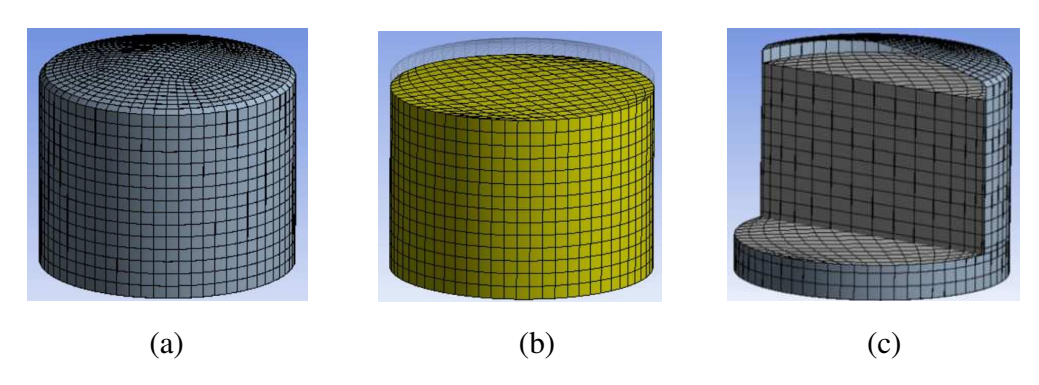


Fig. 5. Meshed 3D CST model including (a) shell wall, (b) internal fluid, and (c) cross section profile

3. Dynamic Analysis Results

The modeling of the dynamic behavior of CST system includes two aspects. One is to simulate fluid movements induced by the ground excitation and the resulting hydrodynamic pressure acting on the tank structure. The other is the modeling of the dynamic response of the tank wall due to both the ground motions and the hydrodynamic pressure. In order to evaluate the dynamic characteristics of this structure, modal analysis was conducted firstly, (Section 3.1), and then nonlinear time history analyses were conducted considering the structure-fluid interaction. (Section 3.2).

3.1 Modal analysis

Generally, modal analysis is used to determine the dynamic characteristics, such as natural frequencies and mode shapes, which are critical in designing a structure subjected to dynamic loading. Linear-elastic small deformation analysis is performed for modal analysis as a first step. According to earlier studies, dynamic behavior of liquid storage tanks is characterized by two predominant modes of vibration, impulsive and convective modes as discussed above (Housner, 1963; Haroun and Housner, 1981). Although it is well known that the first few modes would be adequate to capture the main dynamic response of structure systems, a large number of modes were obtained and analyzed for the simulation of the CST system response. Results from three 2D simplified models show good agreement with the analytical prediction for the minimum natural frequency according to Equation 1, which accounts for the convective response as listed in Tables 2 and 3. The significance of the natural modes is investigated by comparing the mass participation

ratios for each extracted mode. Mass participation percentage for a given mode indicates the contribution of that specific mode to the total dynamic response. For example, Table 2 shows that approximately 24.5 percent of the total dynamic response is contributed by the first mode while the remaining 75.5 percent is dominated by the second model according to Housner (1963) model.

Table 2. Natural frequencies of simplified 2D CST models

Mode number	Natural frequency	Mass participation ratio				
	(Hz)	(%)				
Housner model (1963)						
1	0.24	24.5				
2	7.90	75.55				
Bauer model (1964)						
1	0.35	2.7				
2	0.48	0.4				
3	5.81	96.9				
Haroun and Housner model (1981)						
1	0.24	19.1				
2	4.90 77.7					
3	13.08	3.2				

For the probabilistic seismic risk assessment of nuclear facilities, the estimation of fundamental frequencies of impulsive and convective modes can be determined by the Conservative Deterministic Failure Margin (CDFM) method (Kennedy et al., 1989; Nie et al., 2012). The horizontal impulsive mode natural frequency can be estimated using Equation 1.

$$f_{imp} = \frac{C_{wi}}{2\pi h_w} \sqrt{\frac{127t_s E_s g}{R_t \rho_w}} \tag{1}$$

where E_s is the modulus of elasticity of steel and ρ_w is the density of water. g is the acceleration due to gravity. According to reference (Nie et al., 2012), the harmonic coefficient, C_{wi} , is estimated to be 0.0916 in this study.

The fundamental convective mode frequency is estimated by Equation 2:

$$f_{con} = \sqrt{\frac{0.46(\frac{meter}{sec^2})}{R_t}} \tanh(1.835 \frac{h_w}{R_t})$$
 (2)

Table 3 summarizes the natural frequencies computed for 2D and 3D CST models, and compares the frequencies of convective and impulsive modes with the results determined from Equations 1 and 2. There is good agreement among the convective modal frequencies for all the CST modeling results. However, the natural frequency values of the impulsive mode obtained from various models are slightly different, which is due to assumptions related to the flexibility of the tank wall

and equivalent spring-mass models. Housner's model (1963) includes one convective mass, while both Bauer (1964) and Haroun and Housner's models (1981) are generated with two convective masses and one impulsive mass. The assumptions to compute the values of impulsive masses and their locations are different in each model. Natural frequencies of impulsive mode are also different. Based on the results of modal analyses and time history analyses, Haroun and Housner's model (1981) estimates that the CST structure is more flexibility than the other two models. Figure 6 shows the first two significant mode shapes of three models. The undeformed shape of an empty CST is also shown at the top of the figure for comparison.

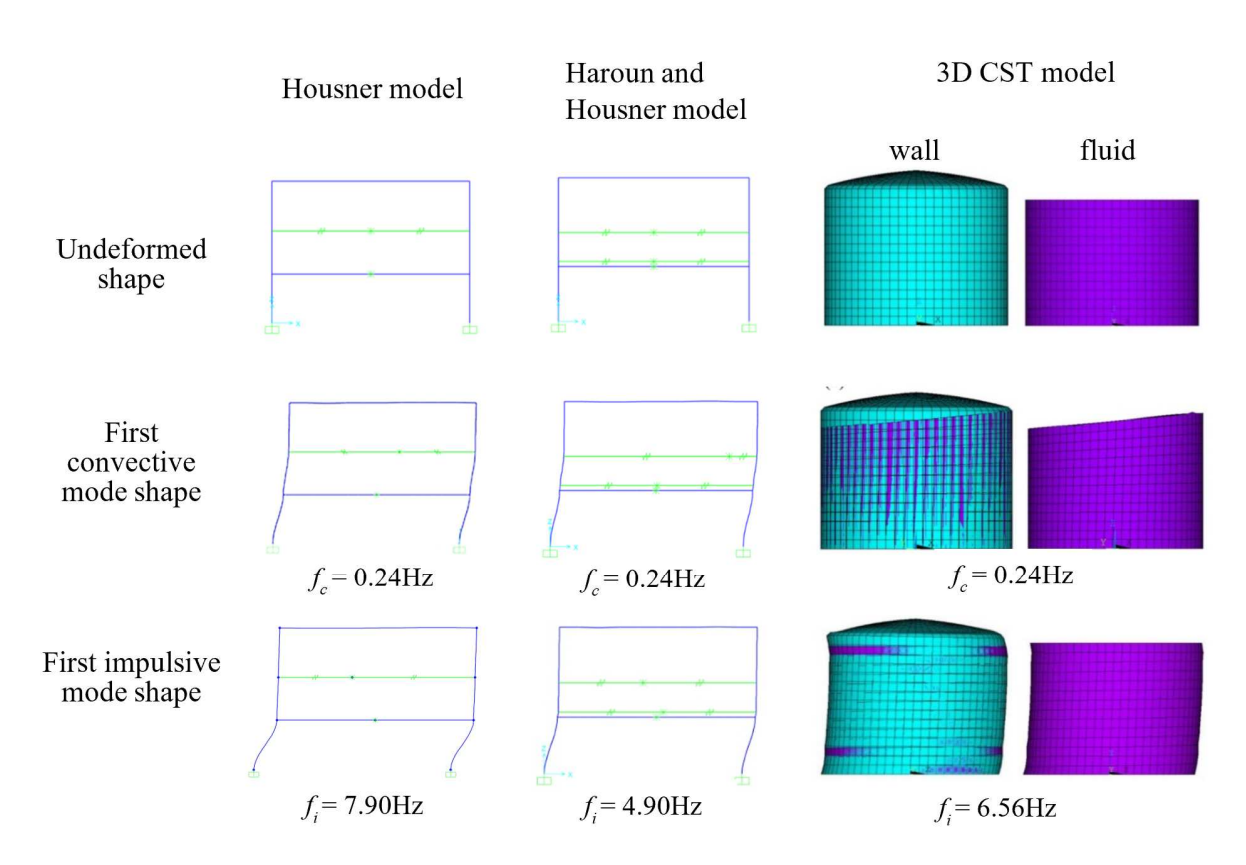


Fig. 6. Modal shapes of 2D and 3D CST models

Table 3 Comparison of natural frequencies (Hz) of 2D and 3D CST models

Mode	Housner (1963)	Bauer (1964)	Haroun and Housner (1981)	Analytical method (Eqs. 1 and 2)	3D FE model
Convective	0.24	0.35	0.24	0.24	0.24
Impulsive	7.90	5.81	4.90	8.89	6.56

3.2 Time History Analysis

To evaluate the response of a structure in SPRA, usually transient dynamic analysis is performed under a set of seismic ground motions (GMs). The loads acting on a structure are of two types: 1) permanent gravity loads with a static response, and, 2) dynamic loads with a time-dependent response. Time history analysis for scenarios involving large loads and potentially large deformations must include the evaluation of water surface movements, base shear, overturning moments, nodal displacements, and resulting stress time history

To illustrate the process for dynamic analysis of CST models, the GM recorded during the El Centro earthquake in 1940 is used (Figure 7). To reduce the computational effort, transient analyses are performed for the first 15 seconds, with a time increment of 0.01 seconds. For this GM record, the peak ground acceleration of 3.417 m/s² (0.313g) is at 2.2 seconds.

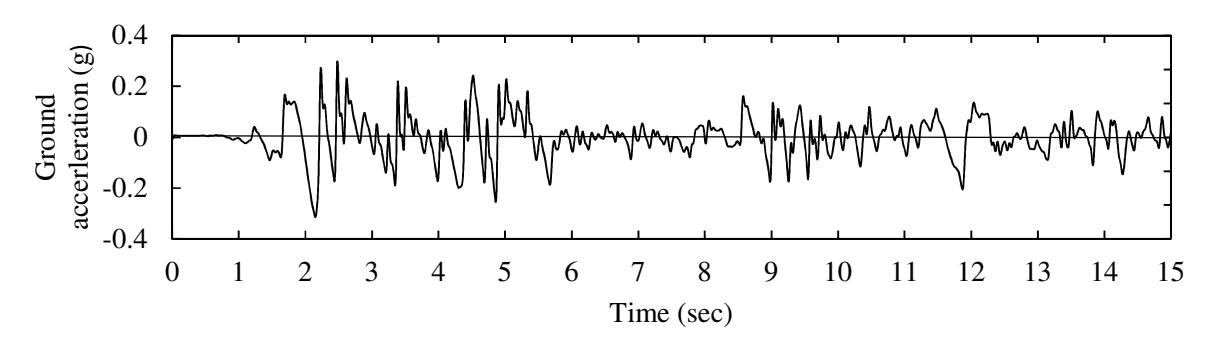
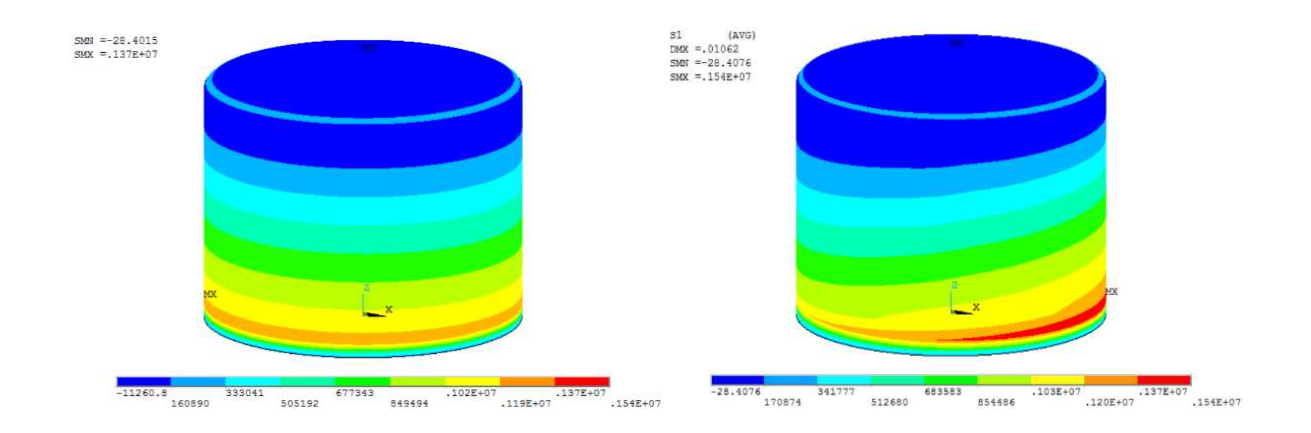


Fig. 7. El Centro time history ground motion input

The hydrodynamic pressure distribution along the height of the wall is calculated for all tank models considered in this study. Figure 8(a) shows the principal stress (σ_1) contours by considering only the gravity loads. As expected, the stress distribution depends on elevation and is independent of azimuth. Figure 8(b) depicts the principal stress distribution on tank walls at the time of peak acceleration (2.2 seconds) when both the axial gravity loads and horizontal ground acceleration are applied. The vertical pressure distribution on the cylindrical tank wall shows the relatively large pressure at a distance about 5 feet above the base of the tank. The maximum stress appears in the direction of input ground motion and gradually diffuses to the upper portion of the tank wall. During the time history analysis, tensile stresses do not exceed the yield stress of the steel material.



(a) (b)

Fig. 8. Principal stress contours due to (a) only gravity load, and (b) combined gravity and lateral seismic loads

The dynamic forces due to seismic ground shaking generate shear forces and overturning moments at the bottom of the tank structure. Due to the static equilibrium requirement, the shear force at the ground level is equal to the sum of the base shear on the bottom plate. Similarly, the total moment at the bottom of the CST equals the sum of the base moments induced by the wall pressures and bending force acting on the tank base. For both 2D and 3D CST models, the overturning moments are obtained at the ground level from the time history analysis considering the reactions at all bottom locations/nodes. Figures 9 and 10 show the calculated time history of overturning moments and base shear for the two 2D simplified models and 3D detailed model, respectively. Maximum values of the base shear and overturning moments are summarized and compared in Table 4.

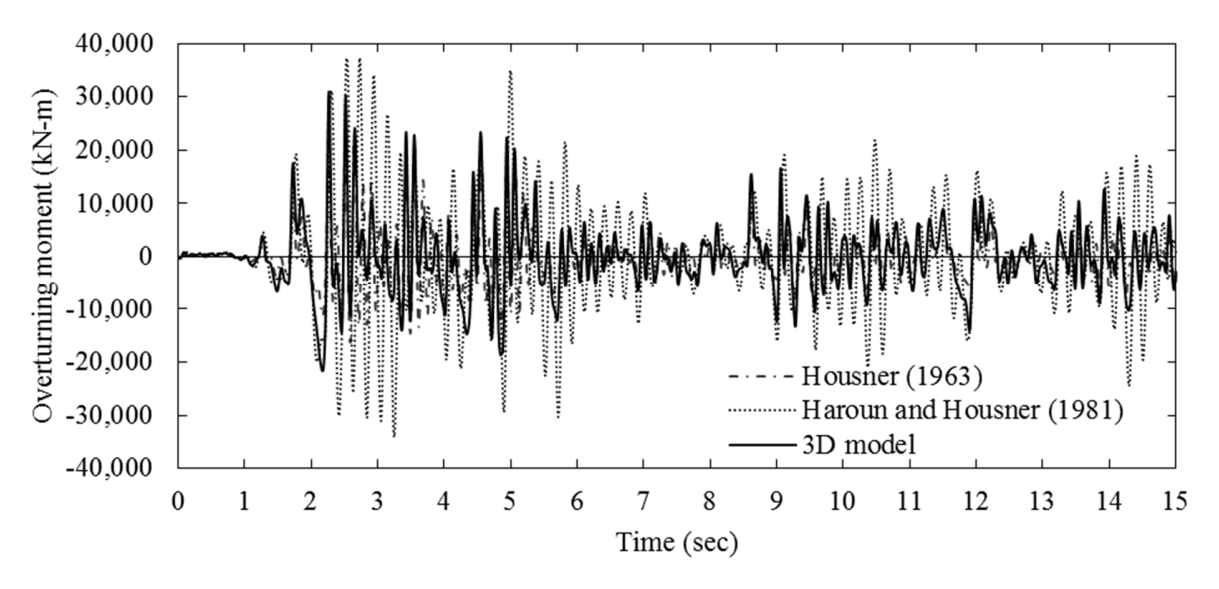


Fig. 9. Time history of overturning moments in 2D and 3D CST models

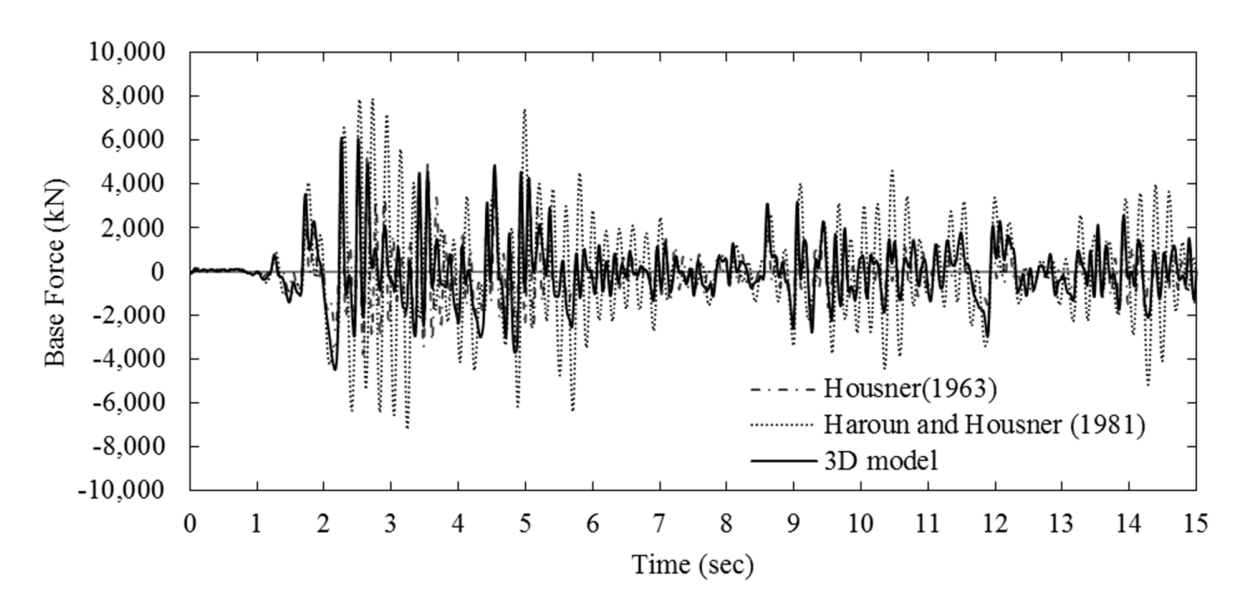


Fig. 10. Time history of base shear in 2D and 3D CST models

Table 4 Comparison of maximum dynamic response of 2D and 3D CST models

Model	Base shear	Overturning moment
	(kN)	(kN-m)
Housner (1963)	5,516	23,198
Haroun and Housner (1981)	7,913	37,242
3D FE model	6,107	29,876
Analytical method (EPRI 6041, 1991)	17,152	41,633

It is observed that the 2D Housner model (1963) yields the smallest shear and overturning moments. Thus, this two-mass model can be non-conservative because it assumes rigid tank walls. For the 3D detailed model, the maximum base shear and overturning moment calculated during time history analysis are 6107 kN and 29,876 kN-m, respectively (Table 4). The maximum response values of the 3D FE model were between those of the Housner's non-conservative model and Haroun and Housner's conservative model with flexible walls.

4. Failure Modes/Limit State Check

During a large earthquake, CST containing liquid may experience significant structural deformations and fluid motion. FSI can lead to nonlinear behavior of materials and buckling of the tank walls. Examples of seismic failure modes of cylindrical storage tanks have been reported and studied (Johnson et al., 2000; Suzuki, 2008). For instance, large axial compressive stresses due to bending of the tank wall can cause "elephant-foot" buckling of the wall. Sloshing of contained fluid not only can increase loads experienced by the wall but also damage the roof of tanks.

Significant base shear force may trigger sliding of the tank. Base uplifting in partially anchored tanks could damage the piping connections, etc. Two of the principal potential failure modes considered in this paper are elephant-foot buckling of the wall due to large axial stress (Section 4.1) plus dynamic hydrodynamic pressure, and sliding failure caused by large shear forces combined with overturning moments at the base of the tank (Section 4.2). The seismic capacities for these potential failure modes are calculated based on methods from several technical reports (EPRI 6041, 1991; EPRI TR-103959, 1994; Hur et al., 2016a).

4.1 Buckling Modes

Although there is no general agreement on the magnitude of the compressive axial stress required to induce buckling of the tank shell, the wall buckling failure mode is typically associated with axial compression (Fan, 2018). The internal pressure exerted by fluid hydrodynamic pressures can significantly influence the buckling strength. Classical theory predicts that instability will occur when the axial compressive stress reaches the ultimate steel strength. The axial compressive stress of tank walls should be less than an allowable steel buckling stress, which is considered for a unidirectional stress state. Under seismic loading, the tank bottom experiences a large compressive stress, together with stress concentration effects and local yielding of the steel shell, which may trigger an elastic-plastic buckling failure. Thus, the elephant-foot mode of buckling may occur at the position of maximum compressive stresses near the tank base. In contrast, the diamond mode of buckling, based on elastic theory of materials, may appear on the weaker parts of the tank wall due to large circumferential compression stresses. The allowable buckling stress is based on the theoretical buckling stress under axial loads in API 650 (2007).

For elastic buckling (diamond buckling) due to compressive stress, the allowable maximum stress, $\sigma_{allowable}$ at the tank wall is determined by Equation 3 (Eurocode 8, 2006)

$$\sigma_{allowable} = 0.6 * E_s \frac{t_s}{R_t} = 200 \text{ Mpa} \qquad . \tag{3}$$

Allowable buckling stress is 200 MPa for the 12.7 mm thick (t_s) and 7.62 m diameter (R_t) CST example analyzed in this research. For elastic-plastic buckling (elephant-foot buckling) due to biaxial stresses, the allowable maximum stress, σ_{be} at the tank wall is estimated by Equation 4 (EPRI 6041, 1991).

$$\sigma_{be} = \frac{0.6E_S t_S}{R_t} \left[1 - \left(\frac{PR_t}{\sigma_{ye} t_S} \right)^2 \right] \left(1 - \frac{1}{1.12 + S_1^{1.5}} \right) \left(\frac{S_1 + \frac{\sigma_{ye}}{250}}{S_1 + 1} \right) = 75.6 \, Mpa$$
 (4)

where σ_{ye} is the effective yield stress of the tank steel shell and equals the yield stress of steel used in this research. P is the maximum tank internal pressure due to fluid near the tank base and is 105 kPa, S_I is calculated by $R_I/400t_s$. Determined by analytical equations, the elephant-foot buckling capacity decreases with the increase of internal pressure, and the diamond buckling capacity increases with the ratio of tank wall thickness over inner radius. Therefore, it can be concluded that at locations near the tank base, where the pressure has maximum values, the tank wall is more vulnerable to elephant-foot buckling. While at the upper levels of tank with less or no internal pressure, diamond type buckling may occur. Figure 11 shows the principal stress distribution due

to hydrodynamic pressure along the height of 3D CST model. During the 15 seconds of transient analysis, the maximum stress is 87.2 MPa.

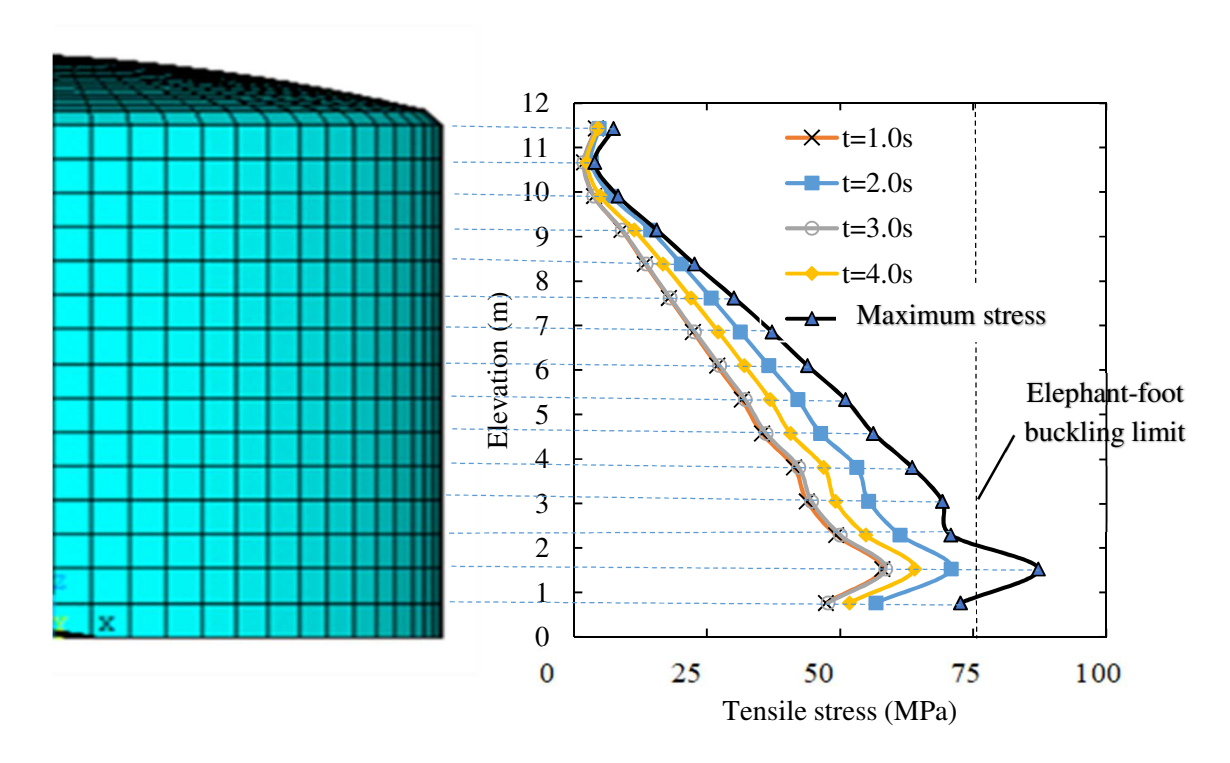


Fig. 11. Maximum compressive stress distribution along the height of the CST wall

4.2 Maximum Overturning Moment at the Bottom

Base shear and overturning moment capacity are calculated by adjusting the assumed neutral axis location gradually until the maximum compressive stress reaches the compressive buckling capacity of the tank wall. The calculations are performed following the methodology presented in the literature (EPRI 6041, 1991; EPRI TR-103959, 1994). The effect of pressure on the tank bottom, known as fluid hold-down forces, is also considered. As shown in Table 4, the calculated maximum dynamic shear and overturning moments in 2D and 3D models are smaller than those predicted from EPRI 6041 (1991) method. In addition, these results confirm the conclusions from comparison of 2D and 3D models during modal analysis, i.e., the rigidity and dynamic properties of the 3D FE model is somewhere between the Housner model and the other 2D (Haroun and Housner's) model. The larger maximum base shears and overturning moments in Haroun and Housner's model indicate that these models have less stiffness than the 3D FE model. Similarly, the smaller base shear and overturning moments in the Housner model implies that the simplified model has a larger stiffness than the 3D FE model.

5. Parametric Analysis

Parametric studies are conducted to investigate the effect of different factors such as mesh size (Section 5.1), and ground motion magnitude on the dynamic response of the 3D CST model (Section 5.2). Convergence studies are carried out to investigate the accuracy and stability of simulations as the number of finite elements increase.

5.1 Sensitivity of Mesh Size

An analytical maximum stress method commonly used for design purposes is adopted to determine an appropriate mesh size for the analysis (Nie et al., 2012). The effects of mesh size of shell element of 3D CST models are evaluated as shown in Figure 12. A series of five cases were considered with different numbers of wall elements in the vertical direction, ranging from 15 to 43 (15 meshed elements is the starting point on the horizontal axis of Figure 12, denoted by 15 E). The bottom plate parallel to the two horizontal directions are divided into 20 meshed elements. The impact on maximum tensile stresses on the tank body is determined from dynamic time history analysis. It is observed that the accuracy of the FE model depends on the number of elements to a small extent. The computation time for each case varies greatly, from less than 4 hours to approximately 14 hours as shown in Figure 12.

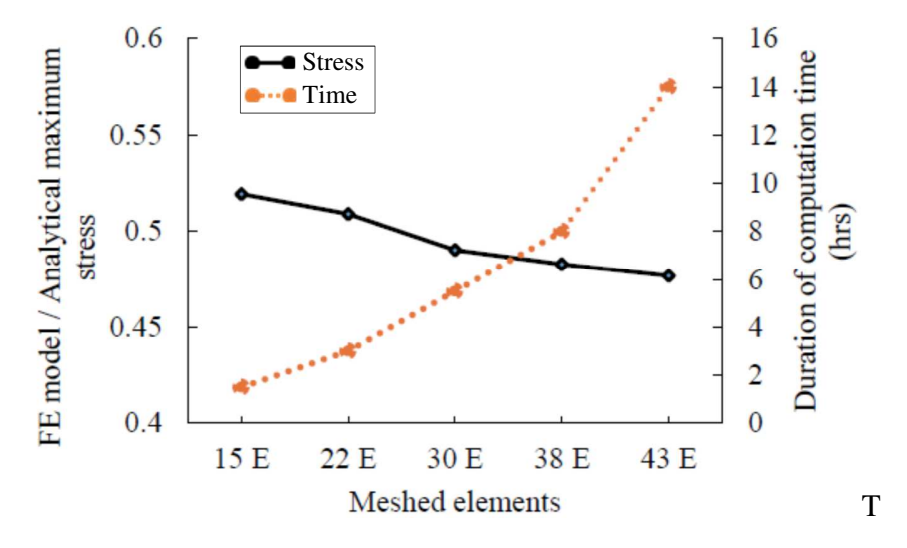


Fig. 12. Sensitivity of maximum stress to mesh size of shell element of CST FE models

5.2 Sensitivity to Magnitude of Ground Motions

The 3D CST model was analyzed under increasing dynamic input magnitude. The El Centro input ground motion accelerations (PGA = 0.3g) were multiplied by two, four, six and ten times for nonlinear analysis of the 3D CST model. Figures 13 and 14 show the calculated maximum displacements and tensile stresses in the tank model at six different times. During the analyses, the maximum ground motion acceleration increased from 0.3g (1×PGA) lateral input shown in Figure 7 to 3.0g (10×PGA) when the input motion was magnified by 10. Figures 13 and 14 show that the maximum displacement and tensile stresses did not increase linearly with increasing ground

motion intensity. This suggests that FSI and nonlinear effects do not necessarily increase the maximum response proportionally with the dynamic input intensity. More nonlinear dynamic analysis of 3D models under different ground motions are necessary to reach more conclusive results.

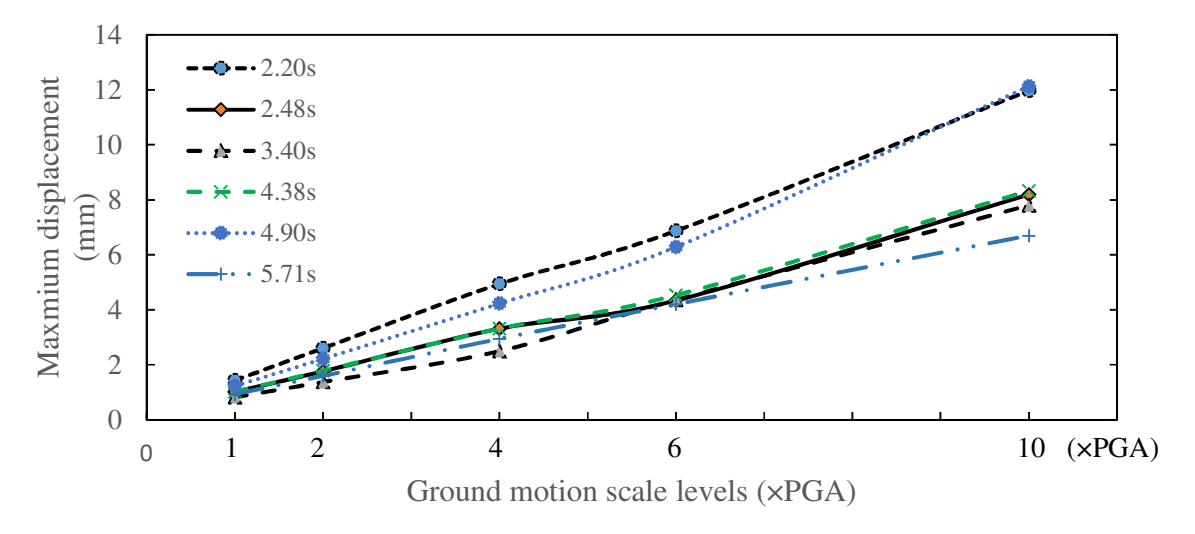


Fig. 13. Maximum calculated displacements in 3D CST models under magnified ground motions

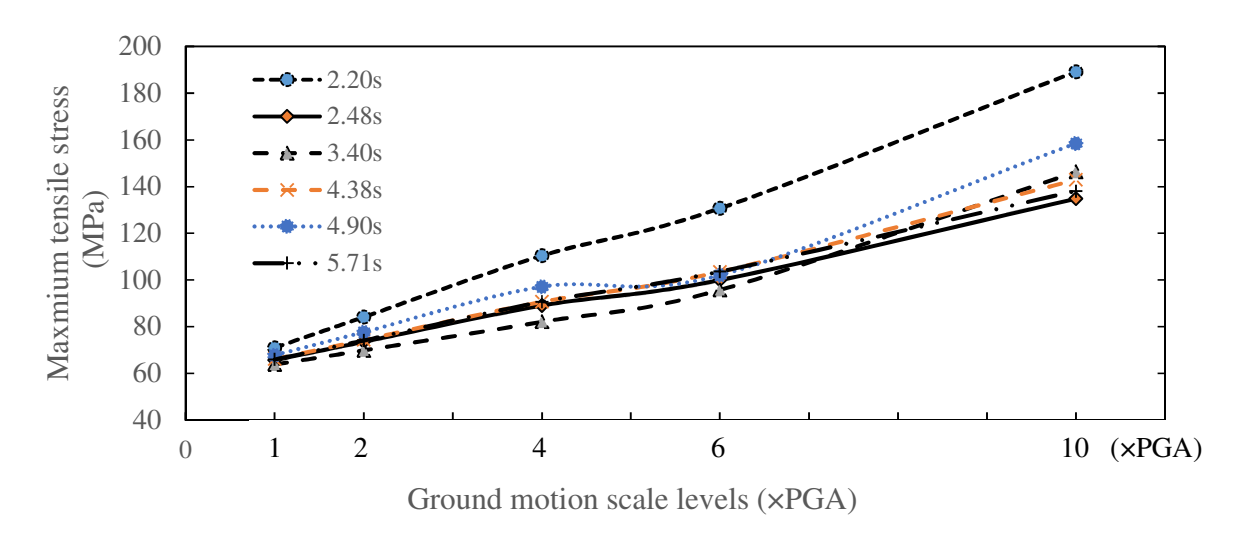


Fig. 14. Maximum calculated tensile stresses in 3D CST models under magnified ground motions

6. Conclusions

In this paper, the seismic performance of CSTs was investigated through modal and time history analyses of simplified 2D and detailed 3D finite element models for the feasibility of using

simplified 2D models for DPRA. Dynamic characteristics and nonlinear seismic behavior of CSTs were evaluated considering the FSI effects. The 3D CST model captures the coupling between the fluid and the tank walls.

Modal analysis was performed to determine the natural frequencies of a partially filled CST considering the FSI effects and sloshing of water near the free surface. The transient dynamic analysis of 2D and 3D CST models were conducted under unidirectional horizontal seismic excitation. Using time history analysis, the failure modes of CSTs were evaluated and the accuracy of the FE model was investigated considering different factors such as mesh size and ground motion intensity on the dynamic response of the 3D water tanks. The following are the main conclusions of this research:

- 1) There is a good agreement between the natural frequencies (0.24 Hz) of convective modes determined from the 2D and 3D CST models. The difference between the frequencies of impulsive modes is equal to or less than 25%.
- 2) Simplified 2D models can be used to quickly estimate the basic dynamic characteristics of CSTs.
- 3) Detailed 3D models provide more realistic simulations of the dynamic response of CSTs considering the FSI and nonlinear behavior of the tank. Depending on the application, an expensive and detailed analysis may be required.
- 4) Dynamic analysis of 3D model showed that under large seismic loads, combined compressive stresses can lead to the elephant-foot buckling mode near the base of the tank. Large circumferential stresses can also lead to the diamond mode of buckling higher on the tank wall.

7. Acknowledgement

This project was funded by the United States Department of Energy Office of Nuclear Energy's Nuclear Energy University Programs (NEUP 13-5132). This support is gratefully acknowledged.

References

ACI 350.3., 2006. Seismic design of liquid-containing concrete structures and commentary. Farmington Hills, MI: American Concrete Institute.

Aldemir, T., 2013. Survey of Dynamic Methodologies for Probabilistic Safety Assessment of Nuclear Power Plants. Annals of Nuclear Energy, 52, 113-124.

Akkose, M., Adanur, S., Bayraktar, A., and Dumanoglu, A. A., 2008. Elasto-plastic earthquake response of arch dams including fluid–structure interaction by the Lagrangian approach. Applied Mathematical Modelling, 32(11), pp.2396-2412.

API Standard 650, 2007. Welded steel tanks for oil storage, 11th Edition. American Petroleum Institute.

ANSYS Mechanical, 2017. Version 17. ANSYS, Inc., Canonsburg, PA. http://www.ansys.com/.

Balendra, T., Ang, K.K., Paramasivam, P. and Lee, S.L., 1982. Seismic design of flexible cylindrical liquid storage tanks. Earthquake Engineering & Structural Dynamics, 10(3), pp.477-496.

Bauer, H. F., 1964. Fluid oscillations in the containers of a space vehicle and their influence upon stability. Washington, D.C.: National Aeronautics and Space Administration.

Brown, K. J., Rugar, P.J., Davis, C.A. and Rulla, T.A., 1995. Seismic performance of Los Angeles water tanks. In Lifeline Earthquake Engineering. ASCE. pp.668-675.

Carluccio A., D., Fabbrocino, G. and Manfredi, G., 2009. FEM analysis of atmospheric tanks under seismic excitation. In Behaviour of Steel Structures in Seismic Areas, STESSA 2009. CRC Press.

Dash, S.R. and Jain, S.K., 2007. Guidelines for seismic design of buried pipelines. IITK-GSDMA Codes.

Di Carluccio, A., Fabbrocino, G. and Manfredi, G., 2008, October. FEM seismic analysis of steel tanks for oil storage in industrial facilities. In Proceedings of the 14th World Conference on Earthquake Engineering.

EPRI NP-6041-M-Rev.1, 1991. A methodology for assessment of nuclear power plant seismic margin. Electric Power Research Institute, Palo Alto, CA.

EPRI NP-5223-SL-Rev.1, 1991. Generic seismic ruggedness of power plant equipment, Electric Power Research Institute, Palo Alto, CA.

EPRI TR-103959, 1994. Methodology for developing seismic fragilities. Electric Power Research Institute, Palo Alto, CA.

Eurocode 8, 20062006. Design of structures for earthquake resistance - Part 4: Silos, tanks and pipelines, European Committee Standardization.

Fan, J., 2018. Modeling of lightly confined reinforced concrete columns subjected to lateral and axial loads. Doctoral Dissertation. The Ohio State University.

Fan, J., Sezen, H., Hur, J., Althoff, E., Denning, R., and Aldemir T., 2017. Structural modeling and seismic analysis of condensate tanks. The 24th International Conference on Structural Mechanics in Reactor Technology, SMiRT 24.

Gradinscak, Marija. 2009, "Liquid sloshing in containers with flexibility." PhD diss., Victoria University.

Hamdan, F.H., 2000. Seismic behavior of cylindrical steel liquid storage tanks. Journal of Constructional steel research, 53(3), pp.307-333.

Haroun, M.A. and Housner, G.W., 1981. Seismic design of liquid storage tanks. Journal of the Technical Councils of ASCE, 107(1), pp.191-207.

Housner, G.W., 1957. Dynamic pressures on accelerated fluid containers. Bulletin of the seismological society of America, 47(1), pp.15-35.

Housner, G.W., 1963. The dynamic behavior of water tanks. Bulletin of the seismological society of America, 53(2), pp.381-387.

Hur, J., Althoff, E., Sezen, H., Denning, R., and Aldemir, T., 2016a. Seismic assessment and performance of nonstructural components affected by structural modeling. Nuclear Engineering and Technology, 49(2), pp. 387-394.

Hur, J., Fan, J., Althoff, E., Sezen, H., Denning, R. and Aldemir, T., 2016b. Development of structural models of a condensate storage tank in nuclear power plants.. 13th International Conference on Probabilistic Safety Assessment and Management, Seoul, Korea.

Jaiswal, O. R., Shraddha Kulkarni, and Pavan Pathak, 2008. A study on sloshing frequencies of fluid-tank system." In The 14th World Conference on Earthquake Engineering, no. 1963.

Johnson G. H., Aschheim M., and Sezen H., 2000. Industrial Facilities. Kocaeli, Turkey Earthquake of August 17, 1999 Reconnaissance Report, Earthquake Spectra, Supplement A to Vol. 16. pp.311-350.

Kennedy, R.P., Murray, R.C., Ravindra, M.K., Reed, J.W. and Stevenson, J.D., 1989. Assessment of seismic margin calculation methods (No. NUREG/CR-5270; UCID-21572). Nuclear Regulatory Commission, Washington, DC (USA). Division of Engineering; Lawrence Livermore National Lab., CA (USA).

Li, Y., Di, Q. and Gong, Y., 2012. Equivalent mechanical models of sloshing fluid in arbitrary-section aqueducts. Earthquake Engineering & Structural Dynamics, 41(6), pp.1069-1087.

Malhotra, P.K., 1997. Seismic response of soil-supported unanchored liquid-storage tanks. Journal of Structural Engineering, 123(4), pp.440-450.

Malhotra, P.K., Wenk, T. and Wieland, M., 2000. Simple procedure for seismic analysis of liquid-storage tanks. Structural Engineering International, 10(3), pp.197-201.

Manos, G.C., 1986. Earthquake tank-wall stability of unanchored tanks. Journal of structural engineering, 112(8), pp.1863-1880.

National Research Council, 1968. The great Alaska earthquake of 1964. National Academies.

New Zealand National Society for Earthquake Engineering and Priestley, M.J.N., 1986. Seismic design of storage tanks: Recommendations of a study group of the New Zealand National Society for Earthquake Engineering. The Society.

New Zealand Standards Association, 2010. NZS3106: The New Zealand Code of Practice for Concrete Structures for the Storage of Liquids.

Nicolici, S. and Bilegan, R.M., 2013. Fluid structure interaction modeling of liquid sloshing phenomena in flexible tanks. Nuclear Engineering and Design, 258, pp.51-56.

Nie, J., Braverman, J., Hofmayer, C., Choun, Y.S., Hahm, D. and Choi, I.K., 2012. A procedure for determination of degradation acceptance criteria for structures and passive components in nuclear power plants. BNL-96775-2012, KAERI/TR-4422/2011.

Rondon, A. and Guzey, S., 2016. Determination of localized stresses in the shell above anchor bolt chairs attachments of anchored storage tanks. Thin-Walled Structures, 98, pp.617-626.

SAP2000, 2016. Version 18. Computers and Structures, Inc., Berkeley, CA. http://www.csiberkeley.com.

Sezen, H., Hur, J., Kose, M.M., Denning, R.S. and Aldemir, T., 2015. Mechanistic and probabilistic seismic assessment of structures and components in nuclear power plants. In SMIRT-23 Conference (Structural Mechanics in Reactor Technology), Manchester, United Kingdom, August 10, 2014.

Sezen, H., Hur, J., Smith, C., Aldemir, T., & Denning, R. 2019. A computational risk assessment approach to the integration of seismic and flooding hazards with internal hazards. Nuclear Engineering and Design, 355, 110341.

Sezen H., Livaoglu R., and Dogangun A., 2008. Dynamic analysis and seismic performance evaluation of above-ground liquid containing tanks. Engineering Structures, 30(3), pp.794-803.

Suzuki, K., 2008. Earthquake damage to industrial facilities and development of seismic and vibration control technology. Journal of System Design and Dynamics, 2(1), pp.2-11.

Veletsos, A.S., 1974, June. Seismic effects in flexible liquid storage tanks. In Proceedings of the 5th world conference on earthquake engineering, Vol. 1, pp.630-639.

Veletsos, A.S., 1984. Seismic response and design of liquid storage tanks. Guidelines for seismic design of oil and gas pipelines system. ASCE, New York, USA, pp.255-370.

Veletsos, A.S. and Auyang, J., 1977. Earthquake response of liquid storage tanks. In Advances in Civil Engineering through Engineering Mechanics, ASCE. pp.1-24.

Veletsos, A.S. and Shivakumar, P., 1997. Tanks containing liquid or solids. A handbook in computer analysis and design of earthquake resistant structures. Computational mechanical publications, pp.725-774.

Veletsos, A.S. and Tang, Y., 1986. Dynamics of vertically excited liquid storage tanks. Journal of Structural Engineering, 112(6), pp.1228-1246.

Veletsos, A.S. and Yang, J.Y., 1976, November. Dynamics of fixed-base liquid storage tanks. In Proceedings of the US–Japan Seminar for Earthquake Engineering Research with Emphasis on

Lifeline Systems, Tokyo, Japan, Japan Society for Promotion of Earthquake Engineering, Tokyo, Japan, pp.317-341.

Wilson, E. L., and Khalvati, M., 1983. Finite elements for the dynamic analysis of fluid--solid systems. International Journal for Numerical Methods in Engineering, 19(11), pp.1657-1668.

Wozniak, R.S. and Mitchell, W.W., 1978. Basis of seismic design provisions for welded steel oil storage tanks. Chicago Bridge & Iron Company. pp.485-501.

Zou, D. and Kong, X., 2000. A simplified seismic response analysis method for cylindrical liquid storage tanks. In Proceedings of the 12th WCEE, Auckland, New Zealand.